Light gluino constituents of hadrons and a global analysis of hadron scattering data

Edmond L. Berger,[1,*] Pavel M. Nadolsky,[2,†] Fredrick I. Olness,[2,‡] and Jon Pumplin[3,§]

[1]*High Energy Physics Division, Argonne National Laboratory, Argonne, Illinois 60439, USA*

[2]*Department of Physics, Southern Methodist University, Dallas, Texas 75275-0175, USA*

[3]*Department of Physics & Astronomy, Michigan State University, East Lansing, Michigan 48824, USA*

(Received 12 June 2004; published 12 January 2005)

Light strongly interacting supersymmetric particles may be treated as partonic constituents of nucleons in high energy scattering processes. We construct parton distribution functions for protons in which a light gluino is included along with standard model quark, antiquark, and gluon constituents. A global analysis is performed of a large set of data from deep-inelastic lepton scattering, massive lepton pair and vector boson production, and hadron jet production at large values of transverse momentum. Constraints are obtained on the allowed range of gluino mass as a function of the value of the strong coupling strength $\alpha_s(M_Z)$ determined at the scale of the Z boson mass. We find that gluino masses as small as 10 GeV are admissible provided that $\alpha_s(M_Z) \geq 0.12$. Current hadron scattering data are insensitive to the presence of gluinos heavier than $\sim$100–150 GeV.

DOI: 10.1103/PhysRevD.71.014007 PACS numbers: 12.38.Bx, 12.60.Jv, 13.87.−a, 14.80.Ly

I. INTRODUCTION

Relatively light strongly interacting fundamental particles may be considered as constituents of nucleons. The nature of these constituents and their experimental effects become evident when the parent hadrons are probed at sufficiently short distances or, equivalently, sufficiently large four-momentum transfer Q. The charm quark $q = c$ and the bottom quark b are treated appropriately as constituents of hadrons in situations in which $Q > m_q$, where m_q is the mass of the heavy quark. Other strongly interacting fundamental particles may exist, as yet undiscovered experimentally, with masses lying somewhere between the bottom- and top-quark masses. One example is a relatively light gluino: a color-octet fermion and the supersymmetric partner of the massless spin-1 gluon. For our purposes, we define a ''light'' particle to have a mass less than 100 GeV. In this paper, we explore the effects that a color-octet fermion would have on the parton distribution functions of nucleons, with a view toward establishing whether the set of hard-scattering data used in global analysis may already place significant constraints on the existence and allowed masses of such states.

In our investigation, we use a light gluino from supersymmetry (SUSY) [1,2] as a concrete example, but our analysis and conclusions should apply as well to the case of a color-octet fermion of whatever origin. As constituents of hadrons, these color-octet fermions share the momentum of the parent hadron with their standard model (SM) quark, antiquark, and gluon partners. The distribution of light-cone momentum fraction x carried by constituents is specified by parton distribution functions (PDFs) as functions of both x and the scale Q of the short-distance hard scattering. The process-independent PDFs are essential ingredients for obtaining normalized predictions of rates for hard-scattering reactions at high energies. A simultaneous analysis of a large body of scattering data (global analysis) provides strong constraints on the magnitude and x dependence of the PDFs.

In perturbative quantum chromodynamics (QCD), the existence of a color-octet fermion and its couplings to the standard model constituents alter the coupled set of evolution equations that governs the functional change of the parton distributions as momentum is varied. Gluinos have different renormalization group properties from those of the quark and gluon constituents, and the contributions of fermions in the color-octet representation are enhanced strongly. Within the context of broken supersymmetry, squarks (scalar partners of quarks) may also be relatively light, particularly those of the third generation, the bottom- and top-squarks [3–6]. In the study reported here, we include a gluino in our PDF analysis, but we neglect possible contributions from other hypothesized supersymmetric states with masses above a few GeV, such as bottom squarks. As explained in Sec. II, the effects of squark contributions on the current data are much less important than those of gluinos. The approximation of retaining only the light gluino contribution simplifies the calculations while retaining most of the relevant physics.

In a global analysis of hadronic data, a large sample of data is studied (about 2000 points) from a variety of experiments at different momentum scales. The data set included in our study is the same as in the recent CTEQ6 [7] study done within the context of the standard model. The data come from deep-inelastic lepton scattering, massive lepton pair and gauge boson production, and hadron jet production at large values of transverse momentum. We apply the methodology of the next-to-leading order (NLO) CTEQ6

*Electronic address: berger@anl.gov

†Current address: High Energy Physics Division, Argonne National Laboratory, Argonne, IL 60439, USA.
Electronic address: nadolsky@hep.anl.gov

‡Electronic address: olness@smu.edu

§Electronic address: pumplin@pa.msu.edu

analysis to explore the compatibility of a light gluino with the large set of hadronic data. Methods developed recently for the analysis of uncertainties of PDFs [8–15] allow us to obtain quantitative bounds on the existence and masses of gluinos from a global analysis. In early PDF analyses within the context of light gluinos [16–18], a gluino with a mass 5 GeV or less was found to be consistent with the data available at that time. A more recent study [19] disfavors a gluino with a mass 1.6 GeV or less. The much larger sample of the data in the modern fit and improved understanding of PDF uncertainties make it possible to derive more precise bounds.

Light superpartners influence the evolution with scale Q of the strong coupling strength $\alpha_s(Q)$. The constraints we obtain on the gluino mass from a global analysis depend significantly on the value of the strong coupling strength $\alpha_s(M_Z)$ that is an ingredient in the global analysis. In Sec. II, we begin with a brief review of the dominant experimental constraints on α_s and consider the changes that may arise if supersymmetric particles and processes are present. Further discussion of experimental constraints on $\alpha_s(M_Z)$ may be found in the appendix. We describe in Sec. II B how we implement the NLO evolution of the PDFs, while including the gluino degree of freedom at leading order (LO). Once supersymmetric particles are admitted, they contribute to hard-scattering processes either as incident partons and/or as produced particles. We therefore specify the hard-scattering matrix elements that describe supersymmetric contributions to the rate for jet production at large transverse momentum. Contributions to jet production at hadron colliders from processes involving supersymmetric partons were considered previously, e.g., in Ref. [20]. In Sec. III, we present and discuss the results of our global fits. The discriminating power of our analysis depends crucially on the inclusion of the Tevatron jet data in the fit. The inclusion of a light gluino in the PDFs removes momentum from the gluon PDF at large x, tending to depress the contribution from SM processes to the jet rate at large E_T. However, the effect is compensated partially by a larger value of $\alpha_s(M_Z)$, slower evolution of α_s that makes $\alpha_s(E_T > M_Z)$ larger than in the standard model, and by contributions to the jet rate from production of SUSY particles in the final state.

Our conclusions are summarized in Sec. IV. We find that the hadron scattering data provide significant constraints on the existence of gluinos whose mass is less than the weak scale $\sim$100 GeV. A large region of gluino parameter space is excluded by the global analysis independently of direct searches or other indirect methods. The quantitative lower bounds we obtain on the gluino mass must be stated in terms of the assumed value of the strong coupling strength $\alpha_s(M_Z)$. For the standard model world-average value $\alpha_s(M_Z) = 0.118$, gluinos lighter than 12 GeV are disfavored. However, the lower bound on $m_{\tilde{g}}$ is relaxed to less than 10 GeV if $\alpha_s(M_Z)$ is increased above 0.120.

II. α_s, PARTON DENSITIES, AND HARD-SCATTERING SUBPROCESSES

The presence of a light gluino $\tilde{g}$ and/or a light squark $\tilde{q}$ modifies the PDF global analysis in three ways. First, the gluino and squark change the evolution of the strong coupling strength $\alpha_s(Q)$ as the scale Q is varied. Second, the gluino and squark provide additional partonic degrees of freedom that share in the nucleon's momentum and affect the PDFs of the standard model partons, e.g., via the channels $g \to \tilde{g}\,\tilde{g}$ and $q \to \tilde{q}\,\tilde{g}$. Third, gluino and squark contributions play a role in the hard-scattering matrix elements for the physical processes for which data are analyzed and fitted. We discuss each of these modifications in the following three subsections.

A. Modified evolution and values of $\alpha_s(Q)$

The expansion of the evolution equation for $\alpha_s(Q)$ as a power series in $\alpha_s(Q)$ is

$$Q\frac{\partial}{\partial Q}\alpha_s(Q) = -\frac{\alpha_s^2}{2\pi}\sum_{n=0}^{\infty}\beta_n\left(\frac{\alpha_s}{4\pi}\right)^n = -\left[\beta_0\frac{\alpha_s^2}{2\pi} + \beta_1\frac{\alpha_s^3}{2^3\pi^2} + \cdots\right]. \quad (1)$$

When supersymmetric particles are included, the first two coefficients in Eq. (1) are (see, e.g., Ref. [21])

$$\beta_0 = 11 - \frac{2}{3}n_f - 2n_{\tilde{g}} - \frac{1}{6}n_{\tilde{f}}, \quad (2)$$

and

$$\beta_1 = 102 - \frac{38}{3}n_f - 48n_{\tilde{g}} - \frac{11}{3}n_{\tilde{f}} + \frac{13}{3}n_{\tilde{g}}n_{\tilde{f}}, \quad (3)$$

where n_f is the number of quark flavors, $n_{\tilde{g}}$ is the number of gluinos, and $n_{\tilde{f}}$ is the number of squark flavors. Equation (2) shows that, to the leading order, one generation of gluinos $\tilde{g}$ contributes the equivalent of three quark flavors to the QCD β function. The effect of one squark flavor is equivalent to one-fourth of the contribution of a quark flavor. In our work, we henceforth neglect the possibility of a light squark contribution to the β function and limit ourselves to the effects of a light gluino. Inclusion of a light bottom squark changes the running of α_s slightly, compatible with current data [22,23]. The modified coefficients β_0 and β_1 for $n_{\tilde{g}} = 1$ and $n_{\tilde{f}} = 0$ are implemented in our numerical calculation to full NLO accuracy.

In our global fit of hadron scattering data, the allowed range of the gluino mass $m_{\tilde{g}}$ depends strongly on the assumed value of the strong coupling $\alpha_s(M_Z)$. Therefore, it is important to understand the current experimental con-

straints on $\alpha_s(M_Z)$ from sources other than hadron scattering data. A combined analysis of all Z pole data within the context of the standard model, carried out by a working group of members of the four CERN Large Electron-Positron Collider (LEP) experiments and the SLAC SLD experiment [24], obtains the value $\alpha_s(M_Z) = 0.1187 \pm 0.0027$.[1] This value is but a shade greater than the often-quoted standard model world-average value $\alpha_s(M_Z) = 0.1183 \pm 0.0027$ [25] obtained from a variety of determinations of $\alpha_s(Q)$ at different momentum scales Q.

The value of $\alpha_s(Q)$ extracted from data in the context of supersymmetric contributions can be different from the value obtained in standard model fits. Some of the assumptions made in a standard model analysis are modified by the presence of the supersymmetric contributions [6,26–28]. A recent estimate of the value of $\alpha_s(M_Z)$ is based on a study of SUSY effects on the hadronic width of the Z, $\Gamma_Z^{\rm had}$ [28]. There are SUSY-QCD effects from subprocesses in which SUSY states are present in loop corrections, e.g., to the partial width for $Z \to b\bar{b}$, and from subprocesses that provide new hadronic final states, such as $Z \to b\tilde{b}^*\tilde{g}$ and $Z \to \bar{b}\tilde{b}\tilde{g}$. The values quoted in Ref. [28] lie in the interval $\alpha_s(M_Z) = (0.118 - 0.126) \pm 0.005$, where the variation in the central value arises from uncertainty in the magnitude of the SUSY contributions. There is also SUSY parameter dependence in the estimate related to the choices of SUSY particle masses and mixing angles. As remarked, this estimate of $\alpha_s(M_Z)$ is related to $\Gamma_Z^{\rm had}$, and other determinations at M_Z may be based on four-jet rates, jet shape variables, and other phenomena. These other determinations may be affected in other ways by the SUSY corrections. Further discussion of the evolution of $\alpha_s(Q)$ in the presence of light supersymmetric states may be found in the appendix.

In a general-purpose CTEQ fit, $\alpha_s(M_Z)$ is fixed at its world-average value, determined from a combination of the τ lepton decay rate, LEP Z pole observables, and other measurements. As discussed above, this value may change in the presence of light superpartners. To explore fully the range of strong coupling strengths compatible with the global fit, we perform a series of fits in which $\alpha_s(M_Z)$ is varied over a wide range $0.110 \le \alpha_s(M_Z) \le 0.150$. We then determine the values of $m_{\tilde{g}}$ and $\alpha_s(M_Z)$ preferred by the global fits. Our choice of the broad range $0.110 \le \alpha_s(M_Z) \le 0.150$ may seem too generous, but it permits construction of the full contour plot shown in Fig. 3, the main result of our paper, entirely from a global analysis of hadron scattering data, independently of other experimental constraints. Were we to enforce an upper value on $\alpha_s(M_Z)$ more in keeping with the range $(0.118–0.126) \pm 0.005$ of Ref. [28], it would not be possible to demonstrate the closure of the contour lines in Fig. 3 at large values of $\alpha_s(M_Z)$.

[1]See Table 16.2 of Ref. [24].

B. Implementation of a gluino in the NLO evolution of parton distributions

In the construction of parton distributions, we include a light gluino and omit squark contributions. A squark enters parton splitting functions only in combination with another rare particle, and these splittings are characterized by smaller color factors than in the gluino case. We incorporate the gluino sector into the PDF evolution package used to build the CTEQ6 unpolarized parton distributions [7].

The standard procedure for extracting parton distribution functions from global QCD analysis is to parametrize the distributions at a fixed small momentum scale Q_0. The distributions at all higher Q are determined from these by the Dokshitzer-Gribov-Lipatov-Altarelli-Parisi (DGLAP) evolution equations [29–31]. The agreement with experiment is measured by an effective χ^2, which can be defined by $\chi^2 = \sum_{\rm expts} \chi_n^2$, or by generalizations of that formula to include published systematic error correlations. The PDF shape parameters at Q_0 are chosen to minimize χ^2 and obtain the ''best-fit'' PDFs.

We choose the starting value Q_0 for the QCD evolution equal to the smaller of the gluino mass $m_{\tilde{g}}$ or charm quark mass m_c. At the scale $Q = Q_0$, the only nonperturbative input distributions are those of the gluons g and light (u, d, s) quarks. Nonzero PDFs of the gluinos and heavy quarks (c, b) are generated radiatively above their corresponding mass thresholds. In the CTEQ6 analysis, Q_0 coincides with the charm quark mass: $Q_0 = m_c = 1.3$ GeV. Therefore, for $m_{\tilde{g}} \ge m_c$ the input scale $Q_0 = 1.3$ GeV is the same as in the CTEQ6 study. We use the CTEQ6 functional forms for the input PDFs of the standard model partons at $Q = Q_0$, but the values of the parameters are varied in order to obtain acceptable fits to the full set of scattering data.

The prescription for Q_0 allows us to investigate the possibility of gluinos lighter than charm quarks ($m_{\tilde{g}} < m_c$). We include fits for gluino masses $0.7 \le m_{\tilde{g}} \le 1.3$ GeV by choosing $Q_0 = m_{\tilde{g}}$. Such superlight gluinos may be generated both via perturbative and nonperturbative mechanisms, and, in principle, an independent phenomenological parametrization must be introduced for the gluino PDF to describe nonperturbative contributions. Our prescription for the region $m_{\tilde{g}} < m_c$ provides a particular model for such an input gluino parametrization, similar in its spirit to the dynamical parton distributions of the GRV group [32], as well as the procedure used in earlier light gluino analyses [18,19].[2]

In the presence of a light gluino, the DGLAP equations must be extended to account for the new processes. The coupled evolution equations take the form

[2]In Ref. [19], the PDFs are obtained from the procedure described here, but at LO and without inclusion of the jet production data, for $m_{\tilde{g}} = 0.5$ and 1.6 GeV.

$$Q^2 \frac{d}{dQ^2}\begin{pmatrix}\Sigma(x,Q^2)\\ g(x,Q^2)\\ \tilde{g}(x,Q^2)\end{pmatrix} = \frac{\alpha_s(Q^2)}{2\pi}\int_x^1 \frac{dy}{y}\begin{pmatrix}P_{\Sigma\Sigma}(x/y) & P_{\Sigma g}(x/y) & P_{\Sigma\tilde{g}}(x/y)\\ P_{g\Sigma}(x/y) & P_{gg}(x/y) & P_{g\tilde{g}}(x/y)\\ P_{\tilde{g}\Sigma}(x/y) & P_{\tilde{g}g}(x/y) & P_{\tilde{g}\tilde{g}}(x/y)\end{pmatrix}\begin{pmatrix}\Sigma(y,Q^2)\\ g(y,Q^2)\\ \tilde{g}(y,Q^2)\end{pmatrix}; \quad (4)$$

$$\Sigma(x,Q^2) = \sum_{i=u,d,s,\ldots}[q_i(x,Q^2) + \bar{q}_i(x,Q^2)]. \quad (5)$$

Here $\Sigma(x, Q^2)$, $g(x, Q^2)$, and $\tilde{g}(x, Q^2)$ are the singlet quark, gluon, and gluino distributions, respectively; $q_i(x, Q^2)$ and $\bar{q}_i(x, Q^2)$ are the quark and antiquark distributions for flavor i. The splitting functions $P_{ij}(x)$ may be found in the literature [33].

The inclusion of a gluino in the evolution equations complicates the calculation substantially. To achieve acceptable accuracy, evolution of the light quarks and gluons must certainly be done at next-to-leading order accuracy. However, without a substantial loss in accuracy, we can simplify the overall calculation by evaluating the gluino contributions to leading order accuracy only. We use the following prescription:

(1) Evolve the ordinary quarks and gluons at NLO [so that the splitting functions $P_{\Sigma\Sigma}$, $P_{\Sigma g}$, $P_{g\Sigma}$, and P_{gg} are evaluated to order $\mathcal{O}(\alpha_s^2)$].
(2) Evolve the gluinos at LO [so that the splitting functions $P_{g\tilde{g}}$, $P_{\Sigma\tilde{g}}$, $P_{\tilde{g}g}$, $P_{\tilde{g}\Sigma}$, and $P_{\tilde{g}\tilde{g}}$ are evaluated to $\mathcal{O}(\alpha_s)$]. In particular, at LO (and in the absence of the squarks), $P_{\tilde{g}\Sigma} = P_{\Sigma\tilde{g}} = 0$.
(3) For the evolution of α_s, use the full NLO [$\mathcal{O}(\alpha_s^2)$] expression, *including* the effect of the gluino.

In this prescription, the evolution is fully accurate to NLO except for the gluino splitting kernels. Were we interested in a process dominated by gluino contributions, we might need a NLO representation of the gluino PDF, $\tilde{g}(x, Q^2)$. However, the impact of the gluino PDF is minimal for the inclusive data in the global analysis, since $\tilde{g}(x, Q^2)$ is much smaller than the quark and gluon PDFs (cf. Figs. 1 and 2). As a result, the gluino plays only an indirect role. Its presence modifies the fit in two ways:

(1) The gluino alters $\alpha_s(Q)$, thereby modifying the evolution of ordinary quark and gluon PDFs.
(2) The gluino carries a finite fraction of the hadron's momentum, thereby decreasing the momentum fraction available to the gluons and standard model quarks.

Regarding item (1), we compute the effects of the gluino correctly by using the exact NLO beta function that includes SUSY effects. Therefore, the only shortcoming of our prescription is with respect to item (2). We describe correctly the NLO mixing between the quarks and the gluons, but the less consequential mixing of the standard model partons and the gluino is correct only to leading order. The LO approximation for gluino splitting is adequate because we assume no *intrinsic* gluino distribution. Consequently, the gluino PDF is present only as a result of evolution, and gluinos contribute to the fitted processes only as a minor contribution to the jet cross section. In the energy range of our interest, the gluinos carry a small fraction ($\lesssim 5\%$) of the proton's momentum. The neglected NLO corrections to this small quantity are further suppressed by a factor of α_s/π. They are comparable in magnitude to the NNLO corrections for the standard model splittings, which are suppressed by α_s^2/π^2. The uncertainty introduced by the omission of the NLO gluino splittings is comparable to that due to the NNLO corrections for other particles, and it may be ignored in the present NLO analysis.

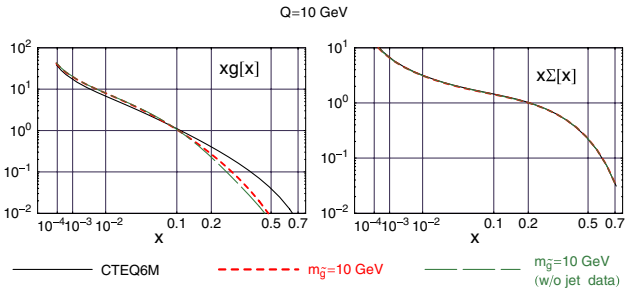

FIG. 1 (color online). The gluon and singlet momentum distributions $xg(x, Q^2)$ and $x\Sigma(x, Q^2)$ are displayed as functions of x at $Q = 10$ GeV with $\alpha_s(M_Z) = 0.118$ and $m_{\tilde{g}} = 10$ GeV. The curves show the conventional CTEQ6M fit (solid) and the LG solutions with (short-dashed) and without (long-dashed) the Tevatron jet data included in the data set.

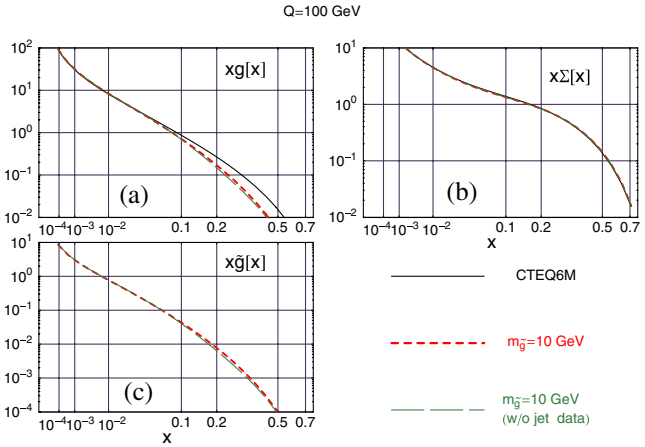

FIG. 2 (color online). The gluon, singlet, and gluino momentum distributions $xg(x, Q^2)$, $x\Sigma(x, Q^2)$, and $x\tilde{g}(x, Q^2)$ are displayed as functions of x at $Q = 100$ GeV with $\alpha_s(M_Z) = 0.118$ and $m_{\tilde{g}} = 10$ GeV. The curves show the conventional CTEQ6M fit (solid) and the LG solutions with (short-dashed) and without (long-dashed) the Tevatron jet data included in the data set.

Figs. 1 and 2 illustrate and support our assumptions. They show the momentum distributions for the gluons, singlet quarks, and gluinos, respectively. In these figures, the strong coupling strength $\alpha_s(M_Z)$ is equal to 0.118 [the value of $\alpha_s(M_Z)$ assumed in the CTEQ6 analysis]. The momentum scale Q is 10 GeV in Fig. 1 and 100 GeV in Fig. 2. The abscissa is scaled as $x^{1/3}$ in these plots of the dependence on the momentum fraction x. The distributions are obtained from the light gluino (LG) fits for $m_{\tilde{g}} = 10$ GeV, with or without the inclusion of the Tevatron jet data. For $xg(x, Q^2)$ and $x\Sigma(x, Q^2)$, we also show the corresponding distributions from the best-fit set CTEQ6M of the CTEQ6 analysis.

With $Q = m_{\tilde{g}} = 10$ GeV, the gluino density $x\tilde{g}(x, Q^2) = 0$. Nevertheless, the effects of gluino contributions on the fit at $Q > 10$ GeV force a change in the gluon and quark distribution functions from their standard model values at $Q = m_{\tilde{g}} = 10$ GeV, as shown in Fig. 1. Once Q is evolved to 100 GeV, Fig. 2 shows a nonzero momentum distribution for the gluinos and a persistent change of the gluon and quark densities from their CTEQ6M standard model values.

The figures demonstrate two important features. First, the magnitude of the gluino distribution is much smaller than the gluon and quark distributions. This large difference justifies the assumptions that contributions are small from scattering subprocesses with initial-state gluinos, and that NLO gluino contributions may be omitted in our analysis.

Second, the presence of the gluino depletes the gluon distribution at $x \gtrsim 0.05$. The effect on the singlet distribution is less pronounced. The gluinos take their momentum (3.7% of the proton's momentum at $Q = 100$ GeV for $m_{\tilde{g}} = 10$ GeV) from the gluons (3.0%) principally, less from quarks (0.7%), independently of whether the Tevatron jet data are included in the fit. Since the jet data at large transverse energy E_T are known to probe the behavior of $g(x, Q^2)$ at large x, i.e., in the region where the depletion of the gluon's momentum is the strongest, we judge that inclusion of the jet data in the fit strengthens the constraining power of the fit.

C. Gluino contributions to hard scattering

Once light superpartners are introduced as degrees of freedom, we must consider their impact on all hard-scattering processes. Their effects can be felt both at tree level and in virtual-loop diagrams. At leading order in perturbation theory, we may consider hard subprocesses initiated by light gluinos or light bottom squarks that are constituents of the initial hadrons, as well as subprocesses in which gluinos or bottom squarks are emitted in the final state. We evaluate SUSY contributions to the hard matrix elements at leading order only for the same reasons that justify the omission of NLO SUSY contributions to the splitting kernels in Sec. II B.

The CTEQ6 fit is performed to data from lepton-nucleon deep-inelastic scattering (DIS), vector boson production (VBP), and hadronic jet production at the Tevatron. We neglect supersymmetric contributions to hard scattering in DIS and VBP. This approximation should be reasonable even if there is a relatively light scalar bottom squark $\tilde{b}$ in the spectrum, as we discuss below. If all squarks are heavy, the gluino contributions to DIS and VBP enter at order $\mathcal{O}(\alpha_s^2)$ and can be safely neglected. If the mass of the lighter of the two bottom squarks is small, e.g. of order 5 GeV, there are contributions to DIS from subprocesses with a $\tilde{b}$ in the initial state. The lowest-order contribution to neutral-current DIS is the sum of the $\mathcal{O}(\alpha_s^0)$ cross section $\gamma^* + \tilde{b} \to \tilde{b}$ and the $\mathcal{O}(\alpha_s^1)$ cross section $\gamma^* + g \to \tilde{b} + \tilde{b}^*$ (with the overlapping contribution of these cross sections subtracted in the collinear kinematic region). We verified that these cross sections are smaller than the analogous cross sections for b quark production, which are themselves suppressed in the inclusive structure functions by the heavy mass and electric charge $-1/3$ of the b quark. The contributions of the heavier of the two bottom squarks would be even further suppressed. Other $\mathcal{O}(\alpha_s^1)$ contributions (such as $\gamma^* + b \to \tilde{b} + \tilde{g}$, $\gamma^* + \tilde{b} \to \tilde{b} + g$, and $\gamma^* + \tilde{g} \to b + \tilde{b}^*$) appear in a combination with small PDFs $b(x, Q^2)$, $\tilde{b}(x, Q^2)$, or $\tilde{g}(x, Q^2)$ and, therefore, are also negligible at the energies probed by the DIS data. Charged-current DIS is insensitive to bottom squarks if the masses of squarks of other flavors are above 100 GeV. For reasons similar to those above, the supersymmetric contributions are small in VBP.

We now consider the influence that gluino subprocesses may have on the rate for jet production at large values of transverse energy E_T. Gluinos are color-octet fermions and, produced in the final state, they materialize as jets. In the standard model, the jets are produced predominantly from quark-quark and quark-gluon scattering, processes enhanced by large valence quark densities at high x. Since the gluino parton density is relatively large only at small values of fractional momentum x and, as illustrated in Figs. 1 and 2, is small even there when compared with the gluon and light-quark densities, each additional gluino in the initial state reduces the relative importance of the subprocess considered. For this reason, we neglect the contributions to the jet rate at large E_T from subprocesses initiated by two gluinos (e.g., $\tilde{g} + \tilde{g} \to g + g$), an approximation that we verified is entirely justified numerically. However, in the interest of completeness, we include two subprocesses initiated by one gluino: $g + \tilde{g} \to g + \tilde{g}$, and $q + \tilde{g} \to q + \tilde{g}$. Subprocesses initiated by gluons and/or light quarks can be important. We include $g + g \to \tilde{g} + \tilde{g}$ via either a direct channel gluon or a cross channel gluino, and $q + \bar{q} \to \tilde{g} + \tilde{g}$ via a direct channel gluon. We can ignore the t channel exchange diagrams that contribute to

$q + \bar{q} \to \tilde{g} + \tilde{g}$. With the possible exception of the bottom squark, the masses of most squarks are so large that the relevant t channel amplitudes are negligible. In the case of bottom squark exchange, the two initial-state partons would be bottom quarks, with small parton densities. For similar reasons, we may also ignore subprocesses such as $q + g \to \tilde{g} + \tilde{q}$.

At the Tevatron $p\bar{p}$ collider, the $q\bar{q}$ partonic luminosity is relatively large in the region of large E_T, and one might expect naively that the subprocess $q + \bar{q} \to \tilde{g} + \tilde{g}$ would increase the jet rate significantly. However, just as for the direct channel gluon subprocess $q + \bar{q} \to q' + \bar{q}'$ in standard QCD, the squared matrix element for $q + \bar{q} \to \tilde{g} + \tilde{g}$ is relatively small.

In our treatment of jet production, we compute the matrix elements for the SUSY-QCD subprocesses at leading order. Working for the most part at values of E_T much larger than the gluino mass, $E_T \gg m_{\tilde{g}}$, we use a zero-mass gluino scheme, neglecting the gluino mass in the hard matrix elements but keeping a finite gluino mass for the gluino threshold condition in α_s, the evolution of the gluino PDF, and the computation of the jet cross sections. We include the gluino matrix elements as additional contributions to the jet rate in the fitting program, adding them to those of the NLO standard model QCD processes $[\mathcal{O}(\alpha_s^3)]$ to obtain constraints from the inclusive jet data. The zero-mass approach handles gluino-initiated processes reasonably well, but it tends to overestimate the contribution from processes with gluinos in the final state (e.g., $g + g \to \tilde{g} + \tilde{g}$ and $q + \bar{q} \to \tilde{g} + \tilde{g}$) in the region near the threshold $E_T \sim 2m_{\tilde{g}}$. We comment further on this point in Sec. III C 1.

As indicated in the previous subsection, inclusion of a light gluino in the PDF set removes momentum from the gluon PDF at large x, tending to depress the contribution from SM processes to the jet rate at large E_T. However, as we show, the effect is compensated partially by a larger value of $\alpha_s(M_Z)$, by slower evolution of α_s that makes $\alpha_s(E_T > M_Z)$ larger than in the standard model, and by contributions to the jet rate from production of SUSY particles in the final state.

III. PRESENTATION OF THE GLOBAL FITS

Our global fits are made to the complete set of data used in the CTEQ6 analysis, for several fixed values of the gluino mass. At this stage of the analysis, we do not impose a value of $\alpha_s(M_Z)$, preferring to determine a range of values directly from the global analysis of hadronic scattering data. We perform fits to the hadronic data with $\alpha_s(M_Z)$ set equal to one of several selected values in the range $0.110 \leq \alpha_s(M_Z) \leq 0.150$. As discussed in Sec. II C, jet production at the Tevatron is the only process among those we include that acquires Born-level contributions from the light gluinos. Most of the figures presented are for fits to the full set of data. To gauge the effect of the jet data, we also show results of additional fits that do not include these data. The numbers of experimental points in the fits with (without) the Tevatron jet data are 1811 (1688).

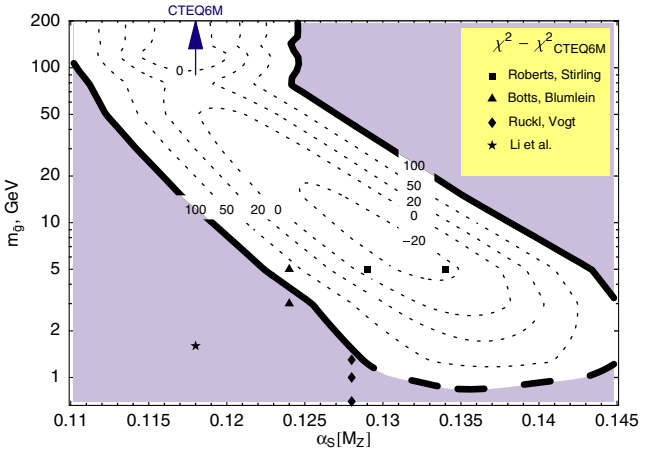

FIG. 3 (color online). A contour plot of $\Delta\chi^2 = \chi^2[\alpha_s(M_Z), m_{\tilde{g}}] - \chi^2|_{\rm CTEQ6M}$ as a function of the strong coupling $\alpha_s(M_Z)$ and gluino mass $m_{\tilde{g}}$. The values of $\Delta\chi^2$ are shown by labels on the corresponding isolines. The shaded region is excluded by the CTEQ6 tolerance criterion. The points corresponding to the earlier PDF fits with a LG [16–19] are denoted by the symbols described in the legend. The solid line marks the $\Delta\chi^2 = 100$ isoline. The dashed completion of this line at the bottom of the contour plot corresponds to fits done with $m_{\tilde{g}} = Q_0 \leq m_c = 1.3$ GeV.

A. Contour plots of $\Delta\chi^2$ vs α_s and $m_{\tilde{g}}$

The principal result of our analysis is shown in Fig. 3. It maps the region of acceptable values of χ^2 in the plane of $\alpha_s(M_Z)$ and $m_{\tilde{g}}$. The contour plot shows the difference $\Delta\chi^2 \equiv \chi^2(\alpha_s, m_{\tilde{g}}) - \chi^2_{\rm CTEQ6M}$, between the value of χ^2 obtained in our LG fit and the standard model result equivalent to the CTEQ6M fit. The point in the plane corresponding to the CTEQ6M fit ($\alpha_s(M_Z) = 0.118$ and $m_{\tilde{g}} \to \infty$) is marked by the arrow.[3] The variation of χ^2 in the neighborhood of the minimum is used to estimate limits of uncertainty.

An overall tolerance parameter T and a condition $\Delta\chi^2 < T^2$ are used in the CTEQ6 analysis to characterize the acceptable neighborhood around the global minimum of χ^2 in the parton parameter space. The quantitative estimate $T = 10$ is obtained from a combination of the constraints

[3]The best-fit value $\alpha_s(M_Z) = 0.117$ in the CTEQ6 fit is slightly below the world-average value $\alpha_s(M_Z) = 0.118$ assumed in the CTEQ6M PDF set.

placed on acceptable fits by each individual experiment included in the fit [7].[4]

According to the tolerance on $\Delta\chi^2$ of the CTEQ6 analysis, a fit is strongly disfavored if $\Delta\chi^2 > 100$. The isoline corresponding to $\Delta\chi^2 = 100$ is shown in Fig. 3 by the solid line. The acceptable fits lie inside a trough that extends from large gluino masses and $\alpha_s(M_Z) = 0.118$ down to $m_{\tilde{g}} \approx 0.8$ GeV and right to $\alpha_s(M_Z) = 0.145$. An even narrower area corresponds to fits with χ^2 close to those in the CTEQ6M fit. We note that χ^2 is better than in the CTEQ6M fit in a small area in which $m_{\tilde{g}} \lesssim 20$ GeV and $\alpha_s(M_Z) \gtrsim 0.125$, with the minimum $\Delta\chi^2 \approx -25$ at $m_{\tilde{g}} = 8$ GeV and $\alpha_s(M_Z) = 0.130$. This negative excursion in $\Delta\chi^2$ is smaller than the tolerance T^2 and should therefore not be interpreted as evidence for a light gluino.

A substantial region of $\alpha_s(M_Z)$ and $m_{\tilde{g}}$ is excluded by the criterion $\Delta\chi^2 < 100$. For $\alpha_s(M_Z) = 0.118$, gluinos lighter than 12 GeV are disfavored. However, the lower bound on $m_{\tilde{g}}$ is relaxed to less than 10 GeV if $\alpha_s(M_Z)$ is increased above 0.120.

In Fig. 3, the positions are marked of the points $\{\alpha_s(M_Z), m_{\tilde{g}}\}$ of the best fits in earlier PDF analyses with a light gluino [16–19].[5] Most of these earlier solutions are excluded by the present data set, with the exception of the fits corresponding to $m_{\tilde{g}} = 5$ GeV and large $\alpha_s(M_Z) = 0.124$, 0.129, and 0.134 [16,17].

Another perspective is provided by a plot of χ^2 vs $m_{\tilde{g}}$ for several fixed values of $\alpha_s(M_Z)$, shown in Fig. 4. The dependence on $m_{\tilde{g}}$ is observed to be quasiparabolic, with a shift of the minimum of χ^2 to lower $m_{\tilde{g}}$ as $\alpha_s(M_Z)$ increases. When $\alpha_s(M_Z)$ is close to the current world-average value of 0.118, the fit prefers a heavy gluino, or no gluino at all. Very light gluinos are strongly disfavored, and the bound $m_{\tilde{g}} > 12$ GeV is obtained for $\Delta\chi^2 < 100$. For $\alpha_s = 0.122$ and 0.124, the corresponding bounds are $m_{\tilde{g}} > 5$ GeV and $m_{\tilde{g}} > 3$ GeV, respectively.

Conversely, for a very large $\alpha_s(M_Z)$ (> 0.127), the pattern is reversed, and lighter gluinos ($m_{\tilde{g}} < 50$ GeV) are preferred. In the transition region of $\alpha_s(M_Z)$ about 0.127, both very light and very heavy gluinos are disfavored, and a gluino mass in the range 10 to 20 GeV yields a slightly better χ^2 than in the CTEQ6M fit. For a very small gluino mass of 1.3 to 5 GeV, the minimum in χ^2 is achieved for $\alpha_s(M_Z)$ about 0.135, while even larger values

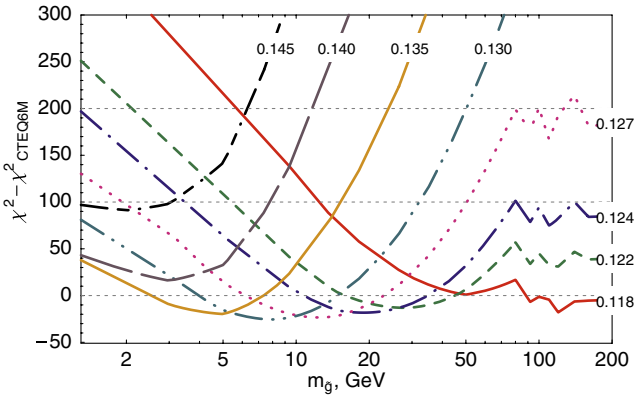

FIG. 4 (color online). Dependence of χ^2 on $m_{\tilde{g}}$ for several fixed values of $\alpha_s(M_Z)$ (denoted by labels on each corresponding line).

of $\alpha_s(M_Z)$ are disfavored as well (cf. the curves for $\alpha_s = 0.140$ and 0.145).

The behavior of χ^2 in Figs. 3 and 4 exhibits irregular structure when the gluino mass lies in the range 50 to ~200 GeV.[6] These gluino masses lie beyond the range of sensitivity of the data sets in the fit, with the exception of the Tevatron jet data at jet transverse energies $E_T > 2m_{\tilde{g}}$. Variations in χ^2 at high gluino masses are caused by an interplay between the gluino mass and individual CDF and DØ jet data points. Contributions from gluinos with masses of 100–140 GeV improve the description of very high-E_T jet events, leading to a dip in χ^2 in this region. Further discussion is found in Sec. III C 1.

In summary, as $\alpha_s(M_Z)$ increases, the window of allowed gluino masses shifts from high to low values. Very large values of $\alpha_s(M_Z)(\gtrsim 0.148)$ can be ruled out for any gluino mass. Gluino masses between 10 and 20 GeV are allowed, as long as $\alpha_s(M_Z)$ is not smaller than ~0.118.

B. Exploration of the light gluino fits

The contour plot in Fig. 3 indicates that excellent fits to the global data can be obtained with a gluino mass below the weak scale, $m_{\tilde{g}} \lesssim 100$ GeV, provided that $\alpha_s(M_Z)$ is allowed to increase above the nominal value $\alpha_s(M_Z) = 0.118$. It is instructive to examine the compensating effects of $\alpha_s(M_Z) > 0.118$ and finite gluino mass on the parton distribution functions themselves.

In Fig. 5, the ratio shown as a dashed line provides a comparison of the gluon distribution $g(x, Q^2)$ at $Q = 15$ GeV and gluino mass $m_{\tilde{g}} = 15$ GeV with $g(x, Q^2)$ in the CTEQ6M fit (without gluinos). The strong coupling α_s at the scale M_Z is chosen to be the same as in the CTEQ6M fit, $\alpha_s(M_Z) = 0.118$. The ratio shows that, as the gluino mass is decreased below the weak scale, $g(x, Q^2)$ is de-

[4]The tolerance $T = 10$ is estimated from the degree of consistency between the various data sets in the global fit. It includes effects due to experimental uncertainty and uncertainties that are of theoretical or phenomenological origin. It is an oversimplification to represent all uncertainties of PDFs and their physical predictions by a single number T. However, given the complexity of the problem, it is unrealistic to be more precise at this stage. The criterion $T = 10$ must be used with awareness of its limitations.

[5]The points corresponding to fits with gluino mass $m_{\tilde{g}} < 0.7$ GeV in Refs. [17–19] are off scale and are not shown.

[6]The irregularities of the contours are smoothed in Fig. 3.

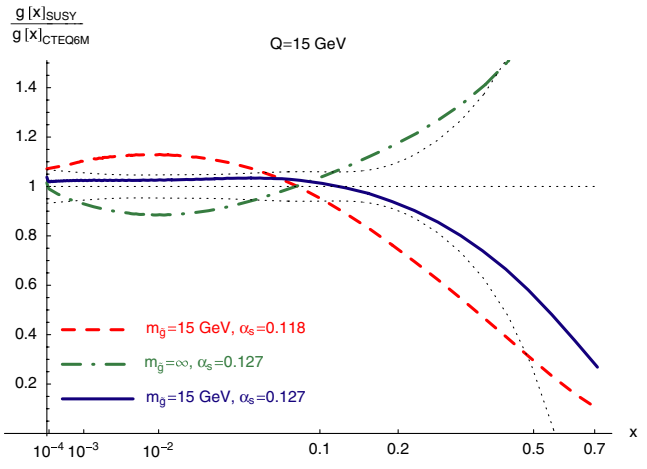

FIG. 5 (color online). Illustration of the compensation in the gluon density that arises between an increase in $\alpha_s(M_Z)$ and a finite gluino mass. Shown are the ratios of the gluon density in the LG solution divided by the CTEQ standard model best fit [$m_{\tilde{g}} = \infty$ and $\alpha_s(M_Z) = 0.118$] at $Q = 15$ GeV. The gluino mass is $m_{\tilde{g}} = 15$ GeV or $m_{\tilde{g}} = \infty$, as specified in the figure. The CTEQ6 uncertainty band is shown by the dotted lines.

pleted at large x and increased at small x. This softening of the gluon distribution follows from the slower evolution of $\alpha_s(Q)$, as well as from the presence of the additional coupling $g \to \tilde{g}\,\tilde{g}$.

For the same $\alpha_s(M_Z)$, the magnitude of $\alpha_s(Q)$ at scales $Q < M_Z$ is smaller in the LG case than in the SM case [cf. Fig. 12(b)]. Correspondingly, PDF evolution is slower in the LG case. To some degree, the effects of the slower backward evolution can be compensated by selection of a larger value of $\alpha_s(M_Z)$. In some range of $m_{\tilde{g}}$ and $\alpha_s(M_Z)$, the effects of a smaller light gluino mass can be offset by a larger value of $\alpha_s(M_Z)$. This statement is illustrated by the dot-dashed curve in Fig. 5. The dot-dashed curve shows the ratio of the gluon density for $m_{\tilde{g}} = \infty$ and $\alpha_s(M_Z)$ increased arbitrarily to 0.127, divided by the SM CTEQ6M result [$m_{\tilde{g}} = \infty$ and $\alpha_s(M_Z) = 0.118$]. The comparison shows that, when $\alpha_s(M_Z)$ is increased, $g(x, Q^2)$ is enhanced at large x and depleted at small x. The solid line in Fig. 5 shows that, by lowering $m_{\tilde{g}}$ below 100 GeV for a fixed $\alpha_s(M_Z)$, we can approximately cancel the effect of increasing $\alpha_s(M_Z)$ at a fixed $m_{\tilde{g}}$. The solid line lies within the band of uncertainty of the CTEQ6 gluon density, indicative of a fit of good quality. The cancellation breaks down at very large $\alpha_s(M_Z)$.

A similar cancellation between the effect of a small $m_{\tilde{g}}$ and increased $\alpha_s(M_Z)$ is apparent in the singlet quark PDF. Consequently, a region exists at small $m_{\tilde{g}}$ and large $\alpha_s(M_Z)$ where the resulting PDFs remain close to those in the CTEQ6M fit. If $\alpha_s(M_Z)$ is allowed to float freely in the fit, one can obtain PDFs similar to the CTEQ6M PDFs for all values of $m_{\tilde{g}}$ above 0.8 GeV. For $m_{\tilde{g}} \gtrsim 150$ GeV, the PDFs are practically the same as in the CTEQ6M fit, indicating that the current inclusive hadronic data are not sensitive to such heavy particles.

C. Impact of various data sets

To appreciate which data are the most restrictive in our fits, we examine the roles played in the fit by the hadronic jet data and other experiments.

1. Tevatron jet data

The Tevatron jet data place important constraints on $m_{\tilde{g}}$. In the absence of the jet data, the lower limit on $m_{\tilde{g}}$ is weaker, with $m_{\tilde{g}} \gtrsim 5$ GeV at $\alpha_s(M_Z) = 0.118$ if the jet data are omitted, but $m_{\tilde{g}} \gtrsim 12$ GeV if the jet data are included.

Comparisons between theory and the inclusive jet data from the CDF Collaboration [34] and the DØ Collaboration [35,36] are shown in Fig. 6 and Figs. 7–9. For these calculations, we set the renormalization scale $\mu = E_T/2$. The results are from a series of fits for fixed $\alpha_s(M_Z) = 0.118$, 0.122, and 0.124. These three values of $\alpha_s(M_Z)$ represent roughly the world-average central value and the values that are approximately 1 and 2 standard deviations larger. The CDF data are rescaled by 1.06 to account for differences in the measured luminosity used by the CDF and DØ Collaborations for the run-I data sample.

The SM CTEQ6M fit with $\alpha_s(M_Z) = 0.118$ provides a good description of the data. For $\alpha_s(M_Z) = 0.118$ and $m_{\tilde{g}} = 15$–25 GeV, the theoretical cross sections fall below

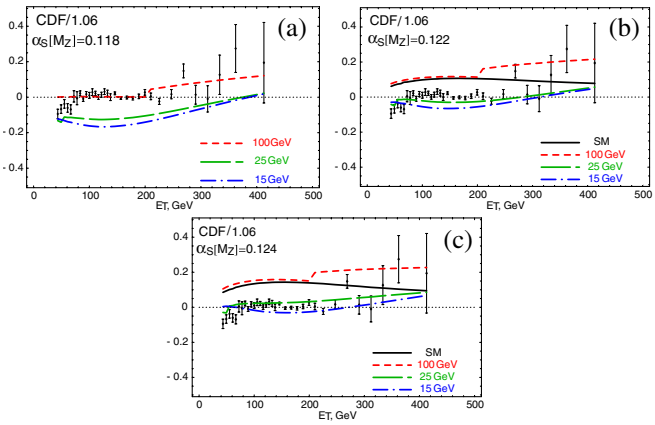

FIG. 6 (color online). Comparison of theoretical predictions with the CDF inclusive jet data. The data points show the ratio (Data-CTEQ6M)/CTEQ6M, where Data denotes the CDF measurements, and CTEQ6M is the SM prediction based on the CTEQ6M PDFs. The curves show the ratio (Theory-CTEQ6M)/CTEQ6M, where the Theory curves are the calculations based on the LG PDFs, for $\alpha_s(M_Z) = 0.118$, 0.122, and 0.124, and gluino masses $m_{\tilde{g}} = \{15, 25, 100\}$ GeV. The solid curves correspond to the SM fits (effectively $m_{\tilde{g}} = \infty$) for the indicated choices of $\alpha_s(M_Z)$. The horizontal scale shows the transverse energy E_T of the jet in GeV units.

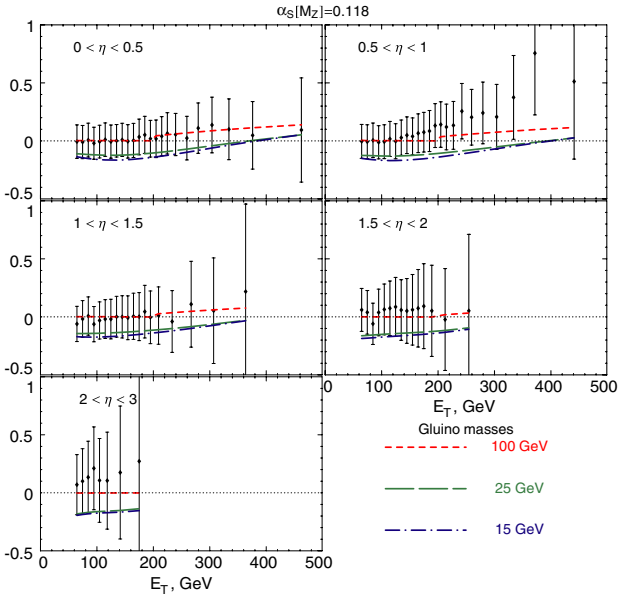

FIG. 7 (color online). Comparison of theoretical predictions with the DØ jet data for $\alpha_s(M_Z) = 0.118$. Shown are (Data-CTEQ6M)/CTEQ6M and (Theory-CTEQ6M)/CTEQ6M, where Data are the DØ measurements, and CTEQ6M and Theory are defined as in Fig. 6. The data are sorted according to the ranges of the jet pseudorapidity η. Curves are plotted for $m_{\tilde{g}} = \{15, 25, 100\}$ GeV.

the data. The primary influences on these results are the presence of the gluino as a parton in the hard-scattering subprocesses and PDFs above the gluino threshold ($Q > m_{\tilde{g}}$); the changes in the evolution of $\alpha_s(Q)$ associated with the SUSY degrees of freedom; and the changes in the gluon PDF that result from these two factors. To distinguish these effects, we first examine Fig. 6(a) in the vicinity of $E_T \sim 200$ GeV. The renormalization scale $Q = E_T/2$ is close to M_Z, so that the value of $\alpha_s(Q)$ is approximately 0.118 for all three values of the gluino mass. Consequently the differences among the curves near $E_T \sim 200$ GeV result only from the presence of the gluino subprocesses or from changes in the gluon PDF. The typical x in the PDFs at this E_T is about $2E_T/\sqrt{S} \sim 0.22$, i.e., in the range affected by the depletion of $g(x)$ for small $m_{\tilde{g}}$ [cf. Figs. 2a and 5]. For $m_{\tilde{g}} = 15$ or 25 GeV, the rate at $E_T \sim 200$ GeV is suppressed by a smaller $g(x, E_T/2)$.

Away from $E_T \sim 200$ GeV, the threshold in the gluino pair production can be seen clearly for $m_{\tilde{g}} = 100$ GeV. It provides an upward shift of the curve for $E_T > 200$ GeV, while the cross section and gluon PDF at $E_T \leq 200$ GeV remain the same as in the standard model. For gluinos lighter than 100 GeV, the E_T dependence of the cross sections away from $E_T \sim 200$ GeV is influenced by both gluon enhancement/depletion and the evolution of $\alpha_s(E_T/2)$. For a given $\alpha_s(M_Z)$, the slower evolution in the presence of a light gluino suppresses the rate at smaller values of E_T and increases the rate for higher E_T. For example, with $m_{\tilde{g}} = 25$ GeV, we find that the ratio of $\alpha_s(Q)$ in the SUSY case to that in the SM is 0.94 at $E_T = 100$ GeV and ~1.07 at $E_T = 400$ GeV, corresponding to factors of 0.88 and 1.14 in rates proportional to α_s^2. In the SUSY case, the gluon PDF is about the same as in the SM or is slightly enhanced for values of $E_T < 100$ GeV ($x < 0.1$) [cf. Figs. 2a and 5], but a significant depletion sets in at

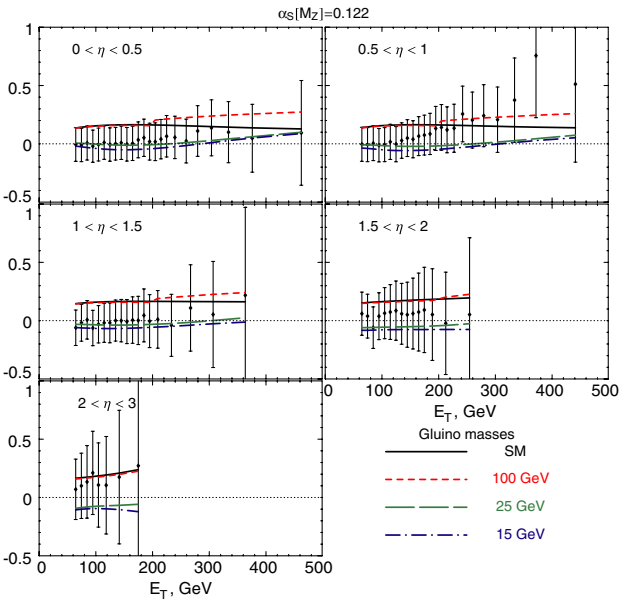

FIG. 8 (color online). Same as in Fig. 7, for $\alpha_s(M_Z) = 0.122$. The solid curves correspond to the SM fit for $\alpha_s(M_Z) = 0.122$.

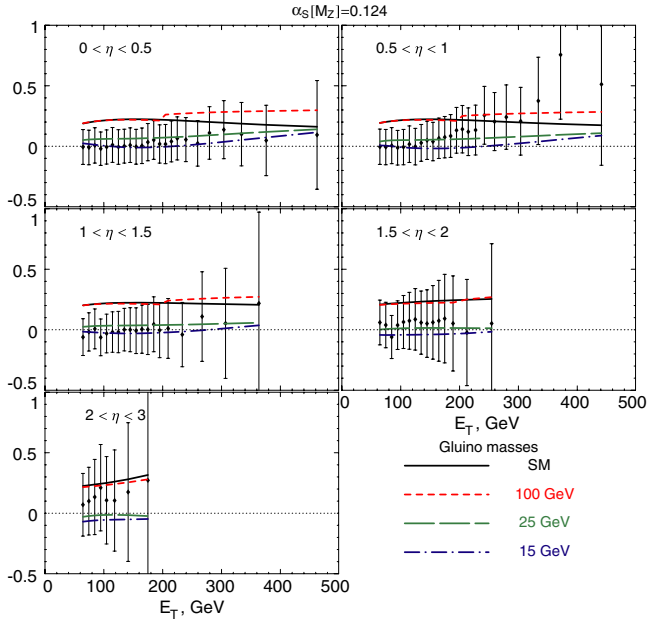

FIG. 9 (color online). Same as in Fig. 7, for $\alpha_s(M_Z) = 0.124$. The solid curves correspond to the SM fit with $\alpha_s(M_Z) = 0.124$.

$x > 0.1$ and grows with E_T. The effects of the changes in $g(x, E_T/2)$ are compensated partially in the cross section by the slower evolution of α_s. The combination of the effects of α_s evolution and changes in the gluon density, along with the contributions from gluino partonic processes, produces a relatively uniform shift in the normalization of the theory curves in most of the energy range, approximately the same as the shift in normalization at $E_T = 200$ GeV. Finally, the effect of a different value of $\alpha_s(M_Z)$ can be appreciated if we compare Fig. 6(b) and Fig. 6(c) with Fig. 6(a). Roughly stated, a different $\alpha_s(M_Z)$ leads to a variation in the overall normalization of the curves, but the general features of the curves remain.

Effects of the depletion of the gluon density can be counterbalanced in a wide range of values of $m_{\tilde{g}}$ by a larger value of $\alpha_s(M_Z)$. The best fits correspond to combinations of α_s and $m_{\tilde{g}}$ near the bottom of the trough in $\Delta\chi^2$ in Fig. 3. For gluinos in the range 10–25 GeV, an acceptable fit is possible if $\alpha_s(M_Z)$ is increased to about 0.124.

Contributions from gluinos increase the jet cross sections at $E_T > 2m_{\tilde{g}}$. A new channel for hard scattering is opened, and the evolution of $\alpha_s(Q)$ is slower. For $\alpha_s(M_Z) = 0.118$, a heavy gluino in the range 100–140 GeV improves agreement of theory with the Tevatron jet data in the high-E_T tail by augmenting the rate of the tightly constrained standard model contributions. Better agreement for $m_{\tilde{g}} = 100$ GeV (dashed line) is visible in the high-E_T region in Figs. 6(a) and 7. Below the gluino threshold, the theory prediction (derived from the fit to the data insensitive to gluino contributions) is identical to the CTEQ6M fit. While χ^2 for the DØ data set is visibly improved (cf. Fig. 10), the reduction of the overall χ^2 is not statistically significant.

Some discussion is in order of the threshold effect seen in the curves for $E_T \approx 2m_{\tilde{g}}$. As remarked above, we calculate observables in a zero-mass variable-flavor-number factorization scheme used in CTEQ6M and other general-purpose PDF sets. In this scheme a gluino, c, or b quark is introduced as an active parton above its respective energy threshold, and the parton masses are neglected in the matrix elements. This method provides a good approximation when the jet energy is much larger than the gluino mass, $\mu^2 = E_T^2/4 \gg m_{\tilde{g}}^2$, but it fails when E_T is of order $2m_{\tilde{g}}$ due to the absence of mass suppression at the threshold. Our bounds on the masses of very light gluinos are unaffected by the zero-mass approximation, but the results shown in Figs. 6–9 overestimate the cross sections with full mass dependence when $m_{\tilde{g}}$ is close to $E_T/2 >$ 25 GeV. This deficiency can be corrected in future analyses, in which NLO SUSY-QCD corrections would also be included and might contribute at a similar level of magnitude. A correct treatment of the gluino threshold could be realized in a scheme with a variable number of massive partons, similar to what has been done in DIS charm and bottom quark production. For the purposes of the present study, we investigate softening of the threshold behavior due to the omitted gluino mass by multiplying the partonic cross sections that involve gluinos by a phase-space inspired factor $\sqrt{1 - 4m_{\tilde{g}}^2/E_T^2}$. The gluino contributions rise more gradually than shown in Figs. 6–9 but, for $m_{\tilde{g}} \sim$ 100 GeV, they achieve their zero-mass asymptotic values at $E_T/2$ about 150 GeV. The overall χ^2 differs by less than ten units from its value in the zero-mass approximation, much smaller than the assumed tolerance $\Delta\chi^2 = 100$. The effect on $\Delta\chi^2$ is even smaller for lower gluino masses.

We conclude that observation of a change in the shape of the jet energy distributions could reveal the existence of superpartners with mass about $E_T/2$. It will be interesting to see whether the possible indication shown in Fig. 10 from the DØ experiment in favor of contributions from gluinos (or other new color-charged fermions) with masses around 100 GeV is sustained in jet data from run-II at the Tevatron.

2. Plots of the data sets vs χ^2

To investigate further the influence of various sets of data, we display the ratios $\chi^2/\chi^2_{\mathrm{CTEQ6M}}$ for individual experiments. Results for $\alpha_s(M_Z) = 0.118$ are shown in Fig. 10 and those for $\alpha_s(M_Z) = 0.135$ in Fig. 11. The choice of the extreme value $\alpha_s(M_Z) = 0.135$ is made to accentuate the effects we want to demonstrate. In Fig. 10, we observe that, in addition to the jet data [sets (n) and (o)], the DIS data from the H1 Collaboration [sets (c) and (d)] and the CCFR F_2 measurement [set (i)] tend to drive the

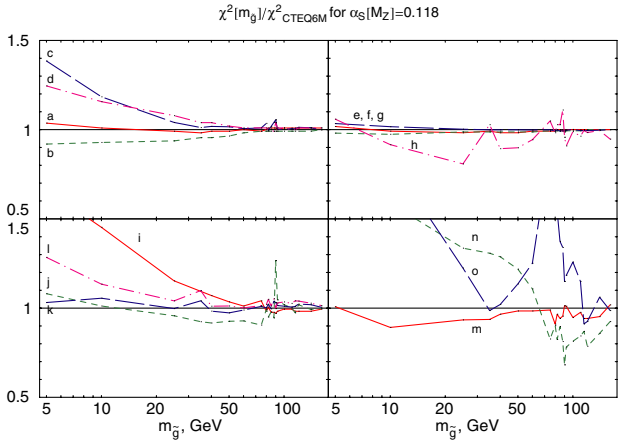

FIG. 10 (color online). Ratios $\chi^2/\chi^2_{\mathrm{CTEQ6M}}$ for individual experiments and $\alpha_s(M_Z) = 0.118$. The curves correspond to the following data sets: (a) BCDMS F_2^p [44]; (b) BCDMS F_2^d [45]; (c) H1 F_2^p (1996/97) [46,47]; (d) H1 F_2^p (1998/99) [48]; (e) ZEUS F_2^p (1996/97) [49]; (f) NMC F_2^p [50]; (g) NMC F_2^d/F_2^p[50]; (h) NMC F_2^d/F_2^p [51]; (i) CCFR F_2 [52]; (j) CCFR xF_3 [52]; (k) E605 muon pair production [53]; (l) CDF lepton asymmetry [54]; (m) E866 muon pair production [55]; (n) DØ jet production [35,36]; and (o) CDF jet production [34].

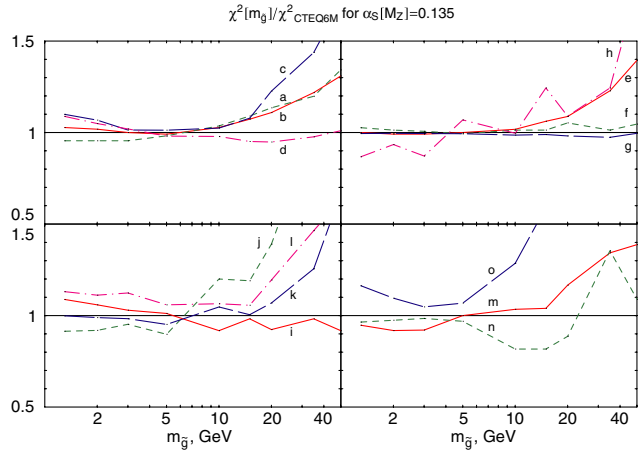

FIG. 11 (color online). Same as in Fig. 10, for $\alpha_s(M_Z) = 0.135$.

gluino mass to large values when $\alpha_s(M_Z) = 0.118$. On the other hand, in Fig. 11 we see that several sets of data are accommodated better with a light gluino if $\alpha_s(M_Z)$ is large.

If $\alpha_s(M_Z)$ is chosen between 0.118 and 0.135, the behaviors of the values of χ^2 for individual experiments follow a mixture of the patterns shown in Figs. 10 and 11. Several data sets disallow very small and very heavy gluino masses, while gluinos in the intermediate mass range are accommodated well by the fit.

D. Section summary and momentum fractions

If $\alpha_s(M_Z)$ is allowed to vary freely, reasonable fits to the global data set are possible for essentially any gluino mass above $\sim$1 GeV. However, if $\alpha_s(M_Z)$ is constrained from other sources, say, τ decay or direct measurements at M_Z, then a global fit to scattering data imposes good constraints on $m_{\tilde{g}}$. This situation is reminiscent of the strong correlation between the gluon PDF and α_s observed in previous analyses of parton densities [37,38]. Similarly, it is not surprising that constraints on the gluino mass are coupled to our knowledge of the gluon PDF (constrained by the hadronic jet data) and $\alpha_s(M_Z)$.

The principal uncertainties on our quoted bounds on the gluino mass arise from neglect of NLO supersymmetric contributions to the PDF evolution (affecting the PDFs at a percent level), neglect of gluino threshold effects and NLO SUSY-QCD corrections in jet production, and the limited precision of the criterion $\Delta\chi^2 < 100$ for the selection of acceptable fits. The lower limit on the gluino mass can be relaxed if the NLO virtual-loop SUSY-QCD corrections enhance the rate of the standard model subprocesses in the Tevatron jet production. These uncertainties can be reduced in future analyses.

We conclude this section with Table I, in which we show the fraction of the proton's momentum carried by its constituents, in both the standard model CTEQ6M fit and in the LG fit with $m_{\tilde{g}} = 15$ GeV and $\alpha_s(M_Z) = 0.122$.

TABLE I. Fractions of the proton's momentum carried by different parton species at $Q = 100$ GeV in the CTEQ6M fit [$m_{\tilde{g}} \to \infty$ and $\alpha_s(M_Z) = 0.118$] and in the LG fit with mass $m_{\tilde{g}} = 15$ GeV and $\alpha_s(M_Z) = 0.122$.

Parton type	CTEQ6M	$m_{\tilde{g}} = 15$ GeV, $\alpha_s(M_Z) = 0.122$
$u + \bar{u}$	25.2	25.4
$d + \bar{d}$	15.4	15.5
$s + \bar{s}$	5.3	5.1
$c + \bar{c}$	3.9	3.6
$b + \bar{b}$	2.5	2.3
Σ	52.3	51.9
g	47.5	44.7
$\tilde{g}$	0	3.2
Total:	100	100

IV. SUMMARY

Our new analysis of the compatibility of a light gluino with inclusive scattering data goes beyond earlier studies [16–19] in a number of aspects. First, the current data are strikingly more extensive than available ten years ago. They cover both small-x and large-Q regions, come from a variety of experiments, and are characterized by high precision. The primary effects of a gluino in the global analysis are changes in the evolution of the strong coupling strength and changes in the evolution of the parton distributions. It is easier to observe these changes in a data sample with large lever arms in Q and x.

Second, in contrast to previous studies, our fit includes the complete set of data from the CTEQ global analysis, including the Tevatron jet production data. The major role of the jet data is to constrain the gluon density at large values of fractional momentum x. The behavior of the gluon density at large x is affected strongly by the presence of the gluinos in the mix. Because they are sensitive to gluons at large x, the jet data enhance the discriminating power of the global fit. When the gluino mass changes, large variations in χ^2 are observed, an influence that can be used to constrain the gluino parameter space. In view of the strong correlations between the gluino mass, $\alpha_s(M_Z)$, and the gluon distribution, the constraints can be determined only after a consistent implementation of SUSY effects throughout all stages of the analysis.

The third new component in our study is a method [7] for quantitative interpretation of uncertainties in parton distributions. With the help of this method, constraints on the acceptable gluino mass can be imposed on the basis of the values of χ^2 obtained in the fits. The main result of the paper is presented in Fig. 3. It shows the region of the gluino masses $m_{\tilde{g}}$ and QCD coupling strengths $\alpha_s(M_Z)$

allowed by the present data. The standard model fit prefers $\alpha_s(M_Z) \approx 0.118$. Gluinos with mass of a few GeV can be accommodated only if $\alpha_s(M_Z)$ is increased. For example, gluinos with mass below 1 GeV are admissible only if $\alpha_s(M_Z)$ is about 0.130 or larger. If one takes into account the effects of a light gluino on the measurement and running of α_s, it is hard (if at all possible) to reconcile such a large value of $\alpha_s(M_Z)$ with both low and high energy electroweak data.

On the other hand, a possibility remains open for the existence of gluinos with mass between 10 to 20 GeV, with a moderately increased α_s [$\alpha_s(M_Z) > 0.119$]. This possibility is even slightly favored over the standard model, according to the χ^2 of our global fit. Tighter constraints will be obtainable in the near future, when new data from HERA and the Tevatron become available. It will be intriguing to see if this hint we may be seeing of physics beyond the standard model is substantiated. Alternatively, we may hope to see evidence for a gluino mass around 100 GeV, as hinted at by our fit to the DØ jet data. A model with light gluinos and bottom squarks [6] is also not incompatible with the results of our PDF analysis.

The constraints we obtain depend on the value of $\alpha_s(M_Z)$. Uncertainties in the value of $\alpha_s(M_Z)$ could be reduced through a consistent determination of $\alpha_s(M_Z)$ from the CERN LEP data in a SUSY-QCD analysis, in which the effects of superpartners are included in the data analyses and Monte-Carlo simulations.

Implementation of the gluino in our study relies only on the knowledge of its strong interactions, which are determined uniquely by supersymmetry. We consider only theoretically clean one-scale inclusive observables. In this sense, our constraint $m_{\tilde{g}} > 12$ GeV for $\alpha_s(M_Z) = 0.118$ should be compared to the constraint $m_{\tilde{g}} > 6.3$ GeV for the same value of α_s from the Z boson width measurement [39]. Tighter constraints on $m_{\tilde{g}}$ were quoted by the searches for traces of gluino hadronization [40,41] and a study of jet shapes [42]. Although important, these constraints are less general, since they involve assumptions about the gluino lifetime or deal with several momentum scales in the jet shape observables. Our study demonstrates the potential of global analysis to independently constrain new physics from hadron collider data.

ACKNOWLEDGMENTS

We thank S. Alekhin, S. Berge, Wu-Ki Tung, and members of CTEQ Collaboration for helpful discussions. P. M. N. and F. I. O. acknowledge the hospitality of Argonne and Brookhaven National Laboratories and Michigan State University, where a portion of this work was performed. Research in the High Energy Physics Division at Argonne National Laboratory is supported by the U. S. Department of Energy, Division of High Energy Physics, under Contract No. W-31-109-ENG-38. The research of P. M. N. and F. I. O. is supported by the U.S. Department of Energy under Grant No. DE-FG03-95ER40908, and the Lightner-Sams Foundation. The research of J. P. is supported by the National Science Foundation under Grant No. PHY-0354838.

APPENDIX: STRONG COUPLING STRENGTH

In this appendix we discuss the quantitative changes that occur in the evolution of the strong coupling strength $\alpha_s(Q)$ in the presence of a light gluino in the spectrum. We consider compatibility of τ decay and LEP Z pole measurements of α_s, which constrain $\alpha_s(Q)$ at low and large momentum scales, respectively.

The measurement of α_s at LEP provides a constraint at scales of order of the Z boson mass M_Z, and the measurement of α_s in τ lepton decay provides a constraint at scales of order of the τ lepton mass m_τ. If the gluino is substantially heavier than the τ lepton, its presence in the spectrum cannot affect the measurement of α_s in τ decay. Therefore,

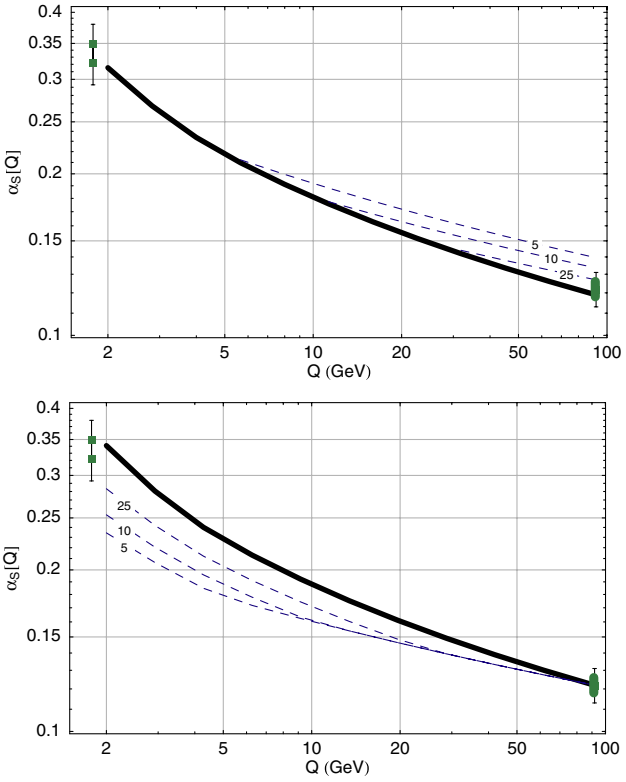

FIG. 12 (color online). Dependence of $\alpha_s(Q)$ on the renormalization scale Q. The three data points shown are $\alpha_s(m_\tau) = 0.35 \pm 0.03$ [43], $\alpha_s(m_\tau) = 0.323 \pm 0.030$ [25], and $\alpha_s(M_Z) = (0.118 - 0.126) \pm 0.005$ [28]. In Fig. 12(a), the average $\alpha_s(m_\tau) = 0.337$ of two experimental values at $Q = m_\tau$ is evolved to higher energies. In Fig. 12(b), the central value $\alpha_s(M_Z) = 0.122$ of the interval at $Q = M_Z$ is evolved to lower energies. The thick solid line represents the standard model evolution in the absence of SUSY effects. The dashed series of curves are generated for gluino masses $m_{\tilde{g}} = 5$, 10, and 25 GeV (shown by the labels on the corresponding curves).

TABLE II. $\alpha_s(M_Z)$ derived by evolution from $\alpha_s(m_\tau) = 0.323 \pm 0.030$ [25] for several gluino masses and in the standard model.

$m_{\tilde{g}}$, GeV	$\alpha_s(M_Z)$
10	0.132 ± 0.004
25	0.125 ± 0.004
50	0.121 ± 0.004
90	0.118 ± 0.003
SM	0.118 ± 0.003

$\alpha_s(Q)$ measured at the scale $Q = m_\tau$ is the same as in the standard model. Its recently quoted values are $\alpha_s(m_\tau) = 0.35 \pm 0.03$ [43] and $\alpha_s(m_\tau) = 0.323 \pm 0.030$ [25]. On the other hand, the measurement of $\alpha_s(Q)$ at $Q = M_Z$ can be affected by light superpartners in the spectrum. The values obtained in standard model analyses may have to be revised [6,26–28].

The τ decay and LEP values of $\alpha_s(Q)$ must be related by the renormalization group equation. Figure 12(a) shows the evolution of $\alpha_s(Q)$ measured in τ decay to the energy of order M_Z for different choices of the gluino mass. According to Eqs. (2) and (3), $\alpha_s(Q)$ evolves more slowly in the presence of light gluinos. Forward evolution of $\alpha_s(m_\tau)$ in the LG case leads to a higher value at $Q = M_Z$ than in the standard model. Evolution of $\alpha_s(m_\tau) = 0.35 \pm 0.03$ results in $\alpha_s(M_Z) = 0.120 \pm 0.003$ in the standard model and 0.135 ± 0.004 for a gluino mass of 10 GeV. Table II lists the values of $\alpha_s(M_Z)$ obtained by evolution from the τ decay value $\alpha_s(m_\tau) = 0.323 \pm 0.030$.

Alternatively, we may evolve α_s measured in Z boson decay backward to energies of order m_τ [Fig. 12(b)]. The resulting $\alpha_s(m_\tau)$ in the LG case is lower than in the standard model. If we use as our starting point the central value $\alpha_s(M_Z) = 0.122$ of the interval $0.118 - 0.126$ found in the SUSY-QCD analysis of Ref. [28], we obtain $\alpha_s(m_\tau) = 0.367$ in the standard model and 0.266 for $m_{\tilde{g}} = 10$ GeV.

For the quoted experimental and theoretical uncertainties, the measurements of α_s at m_τ and M_Z are incompatible at the one-standard deviation (1σ) level *if* the gluino mass is less than about 5.8 GeV. For such gluino masses, the 1σ interval of $\alpha_s(M_Z)$ obtained by evolution from $\alpha_s(m_\tau)$ is above the 1σ interval for the LEP measurement. On the other hand, the τ decay and LEP data do agree at the 1σ level for a gluino heavier than 5.8 GeV, if $\alpha_s(M_Z)$ is at the upper end of the theoretical uncertainty range (i.e., $\alpha_s(M_Z) \sim 0.126 + 0.005$). Lower values of $\alpha_s(M_Z)$ increase the lower bound on $m_{\tilde{g}}$, but gluino masses in the range 10–25 GeV are possible within the uncertainties, as long as the central value of $\alpha_s(M_Z)$ from LEP is not less than about 0.119.

To summarize, bounds on the gluino mass obtained from the global PDF fit depend on the value of $\alpha_s(M_Z)$ assumed in the fit. Gluino masses lighter than 6 GeV cannot agree simultaneously with the results of the global fit, τ decay, and LEP Z pole measurements. Gluino masses as small as 10 GeV—which are slightly favored over the standard model according to the global fit—are consistent with values of $\alpha_s(Q)$ obtained from both τ decay and LEP data.

[1] H. P. Nilles, Phys. Rep. **110**, 1 (1984).
[2] H. E. Haber and G. L. Kane, Phys. Rep. **117**, 75 (1985).
[3] S. P. Martin, hep-ph/9709356.
[4] S. Dawson, hep-ph/9712464.
[5] A. Dedes and H. K. Dreiner, J. High Energy Phys. 06 (2001) 006.
[6] E. L. Berger, B. W. Harris, D. E. Kaplan, Z. Sullivan, T. M. P. Tait, and C. E. M. Wagner, Phys. Rev. Lett. **86**, 4231 (2001).
[7] J. Pumplin, D. Stump, J. Huston, H.-L. Lai, P. Nadolsky, and W.-K. Tung, J. High Energy Phys. 07 (2002) 012.
[8] W. T. Giele and S. Keller, Phys. Rev. D **58**, 094023 (1998).
[9] S. I. Alekhin, Phys. Rev. D **63**, 094022 (2001).
[10] W. T. Giele, S. A. Keller, and D. A. Kosower, hep-ph/0104052.
[11] M. Botje, Eur. Phys. J. C **14**, 285 (2000).
[12] V. Barone, C. Pascaud, and F. Zomer, Eur. Phys. J. C **12**, 243 (2000).
[13] J. Pumplin, D. R. Stump, and W.-K. Tung, Phys. Rev. D **65**, 014011 (2002).
[14] J. Pumplin *et al.*, Phys. Rev. D **65**, 014013 (2002).
[15] D. Stump *et al.*, Phys. Rev. D **65**, 014012 (2002).
[16] R. G. Roberts and W. J. Stirling, Phys. Lett. B **313**, 453 (1993).
[17] J. Blümlein and J. Botts, Phys. Lett. B **325**, 190 (1994); **331**, 450(E) (1994).
[18] R. Rückl and A. Vogt, Z. Phys. C **64**, 431 (1994).
[19] C. S. Li, P. Nadolsky, C.-P. Yuan, and H.-Y. Zhou, Phys. Rev. D **58**, 095004 (1998).
[20] J. L. Hewett, T. G. Rizzo, and M. A. Doncheski, Phys. Rev. D **56**, 5703 (1997); A. Mafi and S. Raby, Phys. Rev. D **62**, 035003 (2000); L. Clavelli, hep-ph/9812340.
[21] M. E. Machacek and M. T. Vaughn, Nucl. Phys. **B222**, 83 (1983).
[22] T. Becher, S. Braig, M. Neubert, and A. Kagan, hep-ph/0112129.
[23] T. Becher, S. Braig, M. Neubert, and A. L. Kagan, Phys. Lett. B **540**, 278 (2002).
[24] ALEPH, DELPHI, L3, OPAL, and SLD Collaborations and the LEP Electroweak Working Group, hep-ex/0312023.
[25] S. Bethke, Nucl. Phys. B, Proc. Suppl. **121**, 74 (2003).

[26] E. L. Berger and L. Clavelli, Phys. Lett. B **512**, 115 (2001).
[27] C.-W. Chiang, Z. Luo, and J. L. Rosner, Phys. Rev. D **67**, 035008 (2003).
[28] Z. Luo and J. L. Rosner, Phys. Lett. B **569**, 194 (2003).
[29] Y. L. Dokshitzer, Sov. Phys. JETP **46**, 641 (1977).
[30] V. N. Gribov and L. N. Lipatov, Yad. Fiz. **15**, 781 (1972).
[31] G. Altarelli and G. Parisi, Nucl. Phys. **B126**, 298 (1977).
[32] M. Gluck, E. Reya, and A. Vogt, Eur. Phys. J. C **5**, 461 (1998), and references therein.
[33] I. Antoniadis, C. Kounnas, and R. Lacaze, Nucl. Phys. B **211**, 216 (1983).
[34] CDF Collaboration, T. Affolder *et al.*, Phys. Rev. D **64**, 032001 (2001).
[35] DØ Collaboration, B. Abbott *et al.*, Phys. Rev. Lett. **86**, 1707 (2001).
[36] DØ Collaboration, B. Abbott *et al.*, Phys. Rev. D **64**, 032003 (2001).
[37] D. W. Duke and J. F. Owens, Phys. Rev. D **30**, 49 (1984).
[38] J. Huston, S. Kuhlmann, H. L. Lai, F. I. Olness, J. F. Owens, D. E. Soper, and W. K. Tung, Phys. Rev. D **58**, 114034 (1998).
[39] P. Janot, Phys. Lett. B **564**, 183 (2003).
[40] DELPHI Collaboration, J. Abdallah *et al.*, Eur. Phys. J. C **26**, 505 (2003).
[41] ALEPH Collaboration, A. Heister *et al.*, Eur. Phys. J. C **31**, 327 (2003).
[42] DELPHI Collaboration, J. Abdallah *et al.*, Eur. Phys. J. C **29**, 285 (2003).
[43] Particle Data Group, K. Hagiwara *et al.*, Phys. Rev. D **66**, 010001 (2002).
[44] BCDMS Collaboration, A. C. Benvenuti *et al.*, Phys. Lett. B **223**, 485 (1989).
[45] BCDMS Collaboration, A. C. Benvenuti *et al.*, Phys. Lett. B **237**, 592 (1990).
[46] H1 Collaboration, C. Adloff *et al.*, Eur. Phys. J. C **13**, 609 (2000).
[47] H1 Collaboration, C. Adloff *et al.*, Eur. Phys. J. C **21**, 33 (2001).
[48] H1 Collaboration, C. Adloff *et al.*, Eur. Phys. J. C **19**, 269 (2001).
[49] ZEUS Collaboration, S. Chekanov *et al.*, Eur. Phys. J. C **21**, 443 (2001).
[50] New Muon Collaboration, M. Arneodo *et al.*, Nucl. Phys. **B483**, 3 (1997).
[51] New Muon Collaboration, M. Arneodo *et al.*, Nucl. Phys. **B487**, 3 (1997).
[52] CCFR Collaboration, W. G. Seligman *et al.*, Phys. Rev. Lett. **79**, 1213 (1997).
[53] E605 Collaboration, G. Moreno *et al.*, Phys. Rev. D **43**, 2815 (1991).
[54] CDF Collaboration, F. Abe *et al.*, Phys. Rev. Lett. **81**, 5754 (1998).
[55] E866 Collaboration, R. S. Towell *et al.*, Phys. Rev. D **64**, 052002 (2001).